Supporting Information

Fused Hexacyclic Thienoquinoids Terminated by Indandione for Low-Bandgap Organic Semiconductors

Yiyang Xu, Tian Du, Yunfeng Deng*, Yanhou Geng

1. Instruments

^{1}H NMR, ^{13}C NMR and ^{19}F NMR spectra were measured by a Bruker 400 MHz spectrometer with chloroform-*d* ($CDCl_3$) and 1,1,2,2-tetrachloroethane-d_2 (CD_2Cl_4) as the solvent and tetramethylsilane (TMS) as internal standard. Matrix-assisted laser desorption ionization time-of-flight (MALDI-TOF) mass spectra was recorded on a Bruker/AutoflexIII Smartbean MALDI mass spectrometer with 2-[(2*E*)-3-(4-*tert*-buthylphenyl)-2-methylprop-2-enylidene] malononitrile (DCTB) as the matrix in a reflection mode. Thermogravimetric analysis (TGA) was carried out on a TA Q50 thermogravimetric analyzer with the heating rate of 10 °C min^{-1} at a nitrogen flow. Differential scanning calorimetry (DSC) was performed by a Perkin-Elmer DSC7 thermal analyzer with a heating/cooling rate of 10 °C min^{-1} under nitrogen. UV-*vis*-NIR absorption spectra were measured with Shimadzu UV3600 plus spectrometer. Cyclic voltammograms (CV, scan rate: 100 mV s^{-1}) were measured on a CHI660E electrochemical analyzer with a three-electrode cell with tetrabutylammonium hexafluorophosphate (Bu_4NPF_6, 0.1 mol L^{-1}) as the supporting electrolyte in anhydrous dichloromethane (CH_2Cl_2). A Pt disk with 2 mm diameter, a Pt wire and a saturated calomel electrode (SCE) were used as working, counter and reference electrodes, respectively. The HOMO and LUMO energy levels were calculated according to the equations: E_{HOMO} = - (4.80 + E_{onset}^{oxi}) eV, E_{LUMO} = - (4.8 + E_{onset}^{red}) eV in which E_{onset}^{oxi} and E_{onset}^{red} represent the oxidation and reduction onset-potentials against the half potential of Fc/Fc^+ (E^o = 0.42 eV). Atomic force microscopy (AFM) measurements were carried out in tapping mode on a Bruker MultiMode 8 atomic force microscope. Density functional theory (DFT) calculated frontier molecular orbital (FMO) distribution and time-dependent DFT (TD-DFT) were conducted by Gaussian 09 with B3LYP/6-31G (d, p) basis set.[1-3] For simplifying, the side chains were replaced as methyl groups. Natural orbital occupation number (NOON) calculations were done by spin unrestricted UCAM-B3LYP/6-31G (d, p) method and the diradical character (y_0) was calculated according to Yamaguchi's scheme: $y_0 = 1 - (2T/(1 + T^2))$, and $T = (n_{HOMO} - n_{LUMO})/2$ (n_{HOMO} is the occupation number of the HOMO, n_{LUMO} is the

occupation number of the LUMO).[4,5] NICS values were calculated (B3LYP/6-31G (d, p)) using the standard GIAO procedure. The charge transfer integrals for the molecular dimer extracted from the experimental crystal structures were calculated at M06-2X/Def2-SVP level in the CT module of NWchem package.

2. Organic thin-film transistors (OTFTs) fabrication and measurements

The charge transport properties of the molecules were characterized using top gate/bottom contact (TG/BC) OTFTs. Highly n-doped silicon wafers covered with a 300 nm thick thermally grown SiO_2 layer were used as substrates. The substrates were washed by an ultrasonic cleaner with deionized water, acetone and isopropanol, respectively, and then dried under a nitrogen flow and heated at 120 °C for 10 min. Au (~30 nm) was deposited on the silicon substrate as source and drain electrodes with shadow mask of W/L = 112 (W = 5600 μm, L = 50 μm). $Ba(OH)_2$ in methanol (2 mg mL^{-1}) was spin-casted at 5000 rpm for 90 s and annealed at 60 °C for 5 min on silicon substrate deposited with Au. Subsequently, the semiconductor films were prepared by spin-coating of the chloroform solutions with a concentration of 5 mg mL^{-1}, followed by annealing 120 °C for 10 min. As the dielectric, Cytop was spin-casted at 2000 rpm for 2 min and annealed at 100 °C for 40 min. Finally, Al (80 nm) was vacuum-evaporated as the gate electrode. OTFT devices were measured under ambient conditions with Keysight B1500A source/measure units. Saturation mobilities were calculated according to equation: $\mu_{sat}(V_G) = \frac{\partial I_{D,\,sat}}{\partial V_G} \cdot \frac{L}{WC_i} \frac{1}{(V_G - V_T)}$.

3. Supplementary Data

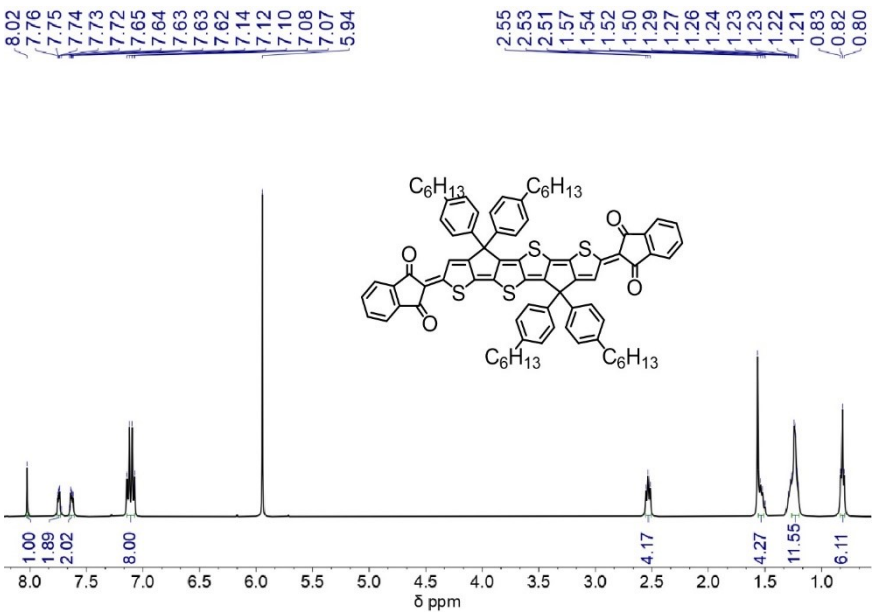

Figure S1. ^{1}H NMR spectrum of **Q4T** (400 MHz, $C_2D_2Cl_4$).

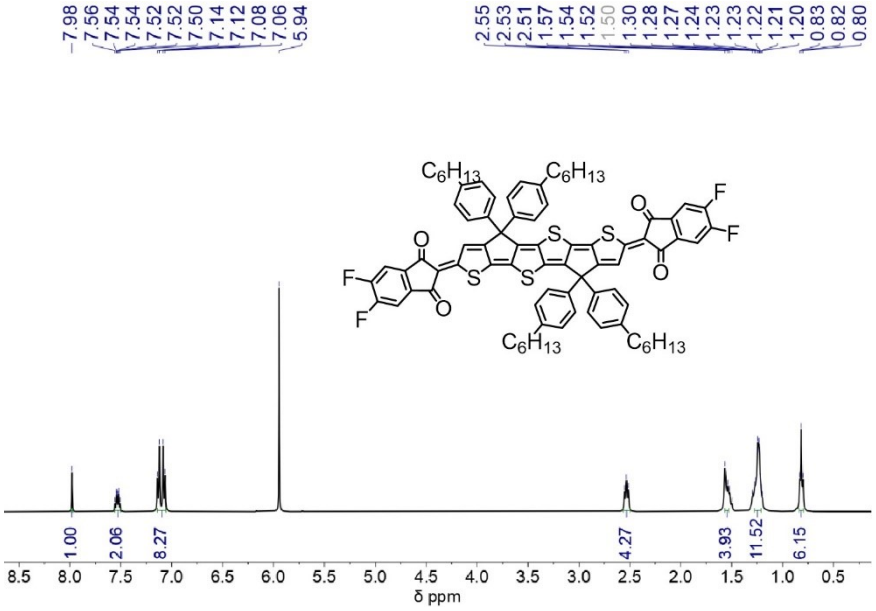

Figure S2. ^{1}H NMR spectrum of **Q4T-4F** (400 MHz, $C_2D_2Cl_4$).

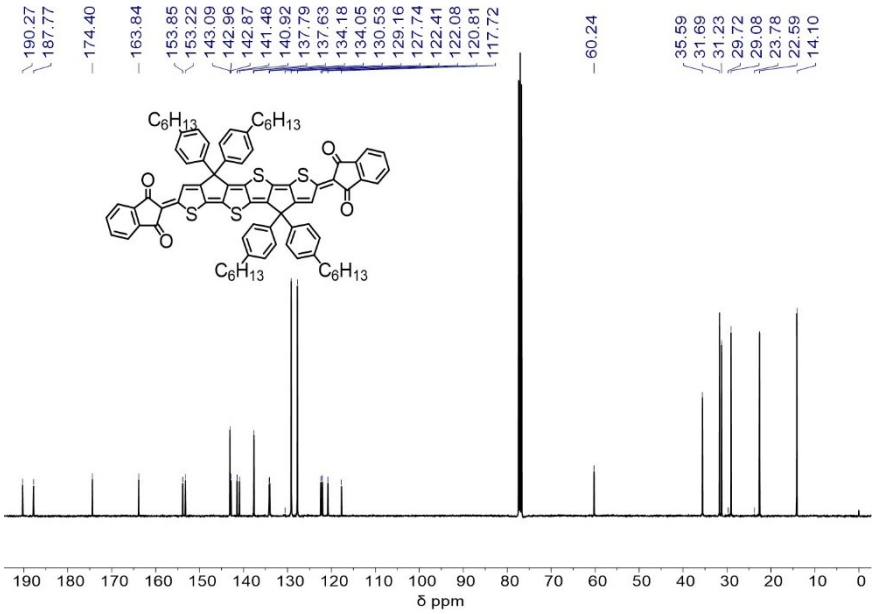

Figure S3. ^{13}C NMR spectrum of **Q4T** (100 MHz, $CDCl_3$).

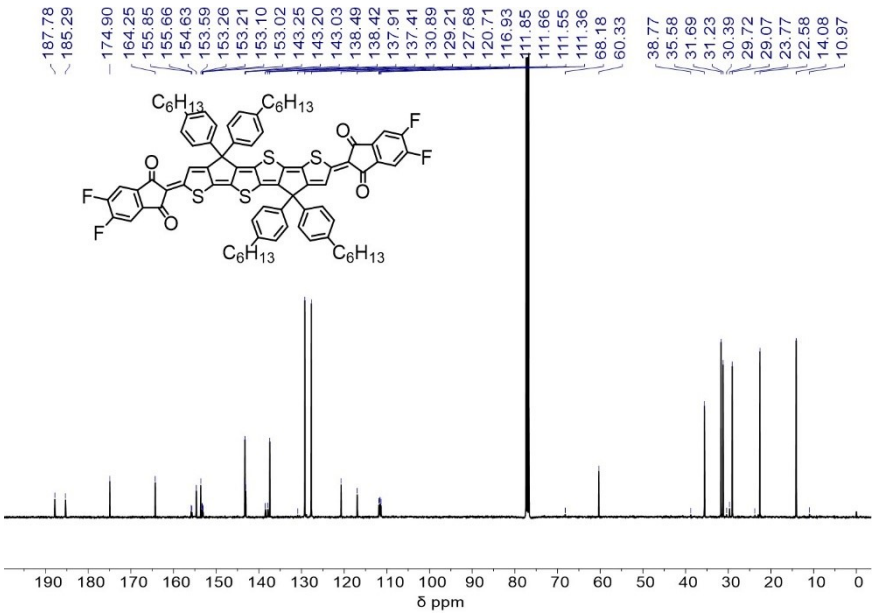

Figure S4. ^{13}C NMR spectrum of **Q4T-4F** (100 MHz, $CDCl_3$).

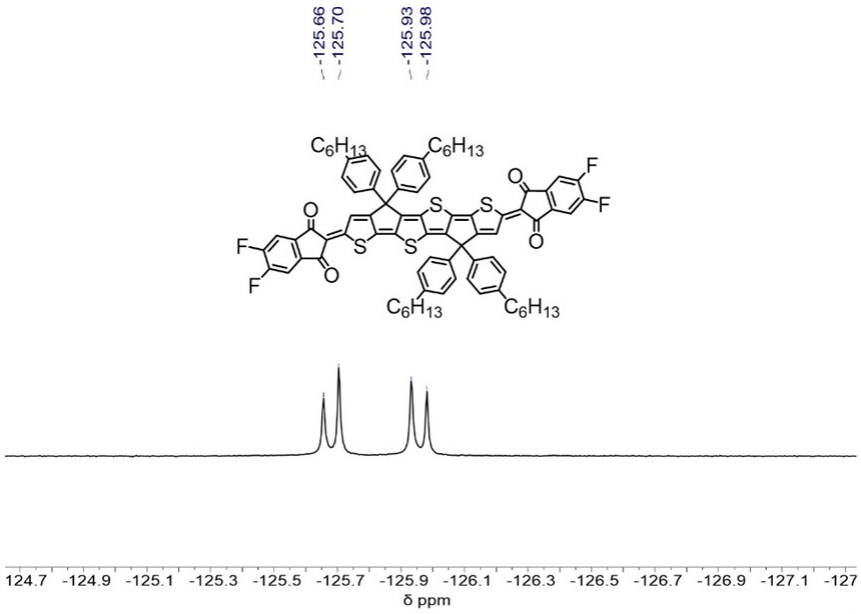

Figure S5. ^{19}F NMR spectrum of **Q4T-4F** (376 MHz, $CDCl_3$).

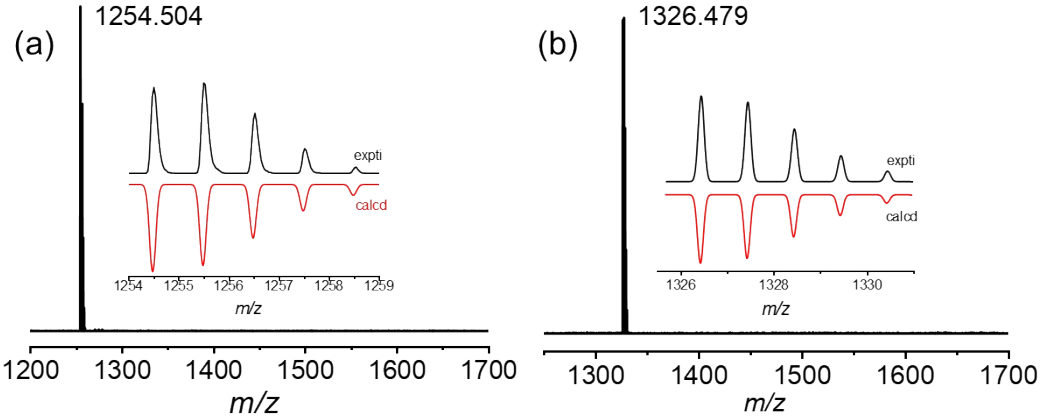

Figure S6. High-resolution MALDI-TOF mass spectra of (a) **Q4T** and (b) **Q4T-4F**.

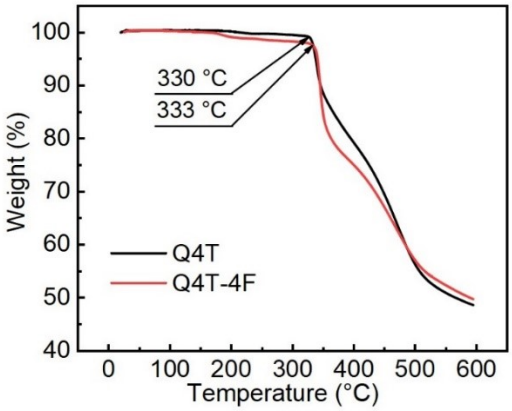

Figure S7. TGA curves of **Q4T** and **Q4T-4F** in N_2 with a heating rate of 10 °C min^{-1}.

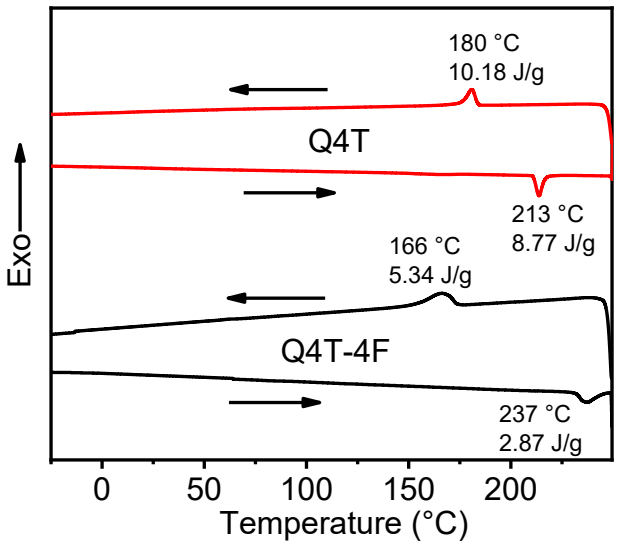

Figure S8. DSC curves of **Q4T** and **Q4T-4F** in N_2 with a heating/cooling rate of 10 °C min^{-1}.

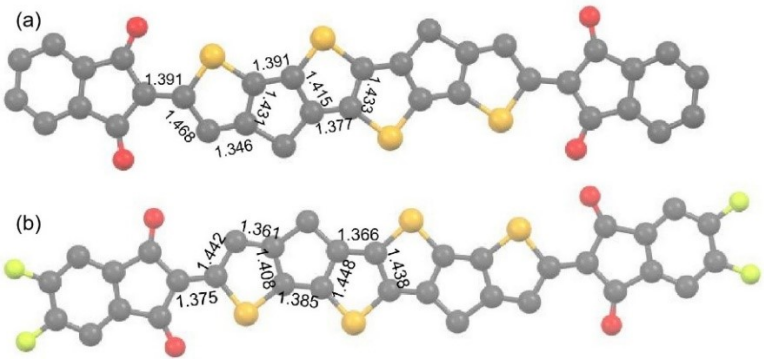

Figure S9. The bond lengths of **Q4T** and **Q4T-4F**.

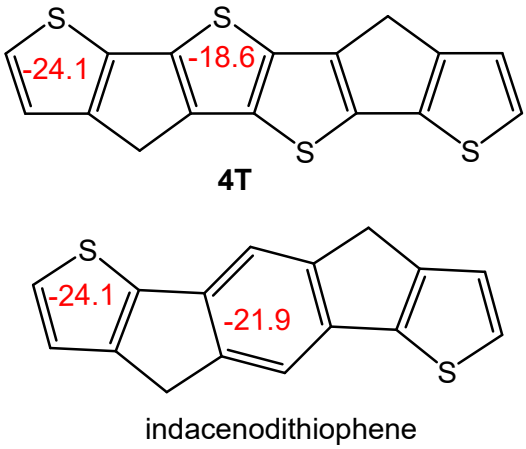

Figure S10. The NICS(1)zz values of **4T** and indacenodithiophene.

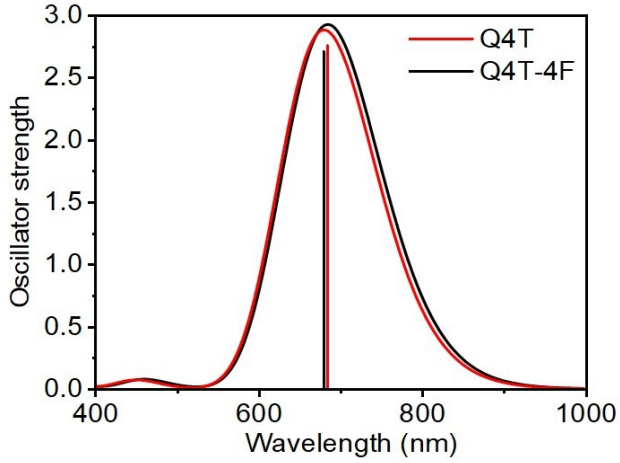

Figure S11. The TD-DFT calculated absorption of **Q4T** and **Q4T-4F**.

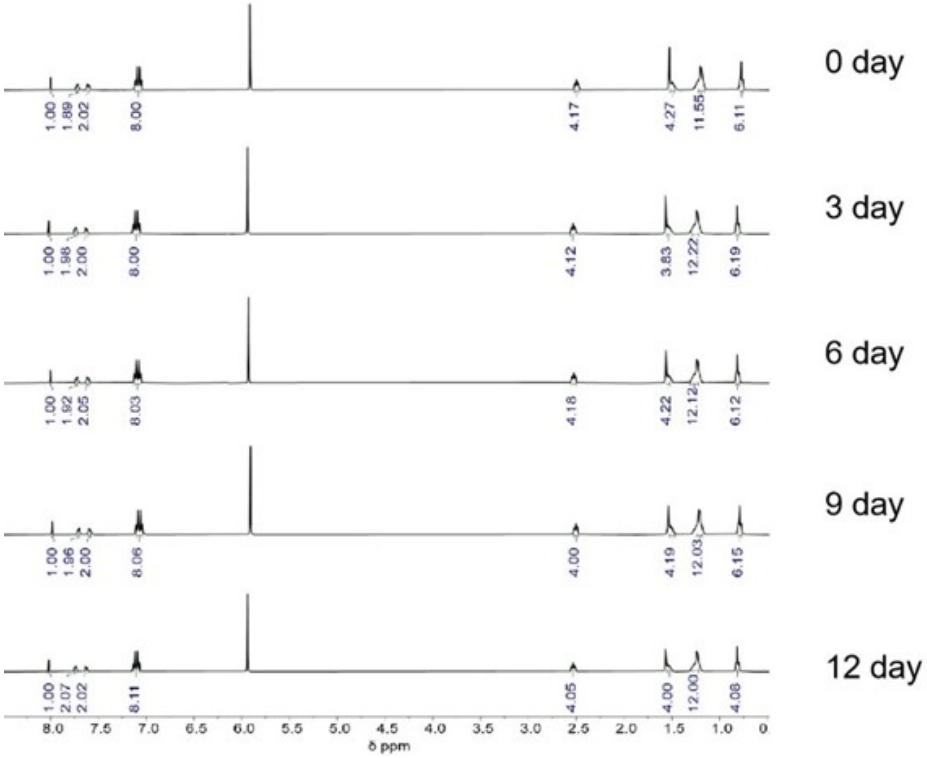

Figure S12. Variable-time ^{1}H NMR spectra of compound **Q4T** (400 MHz, $C_2D_2Cl_4$).

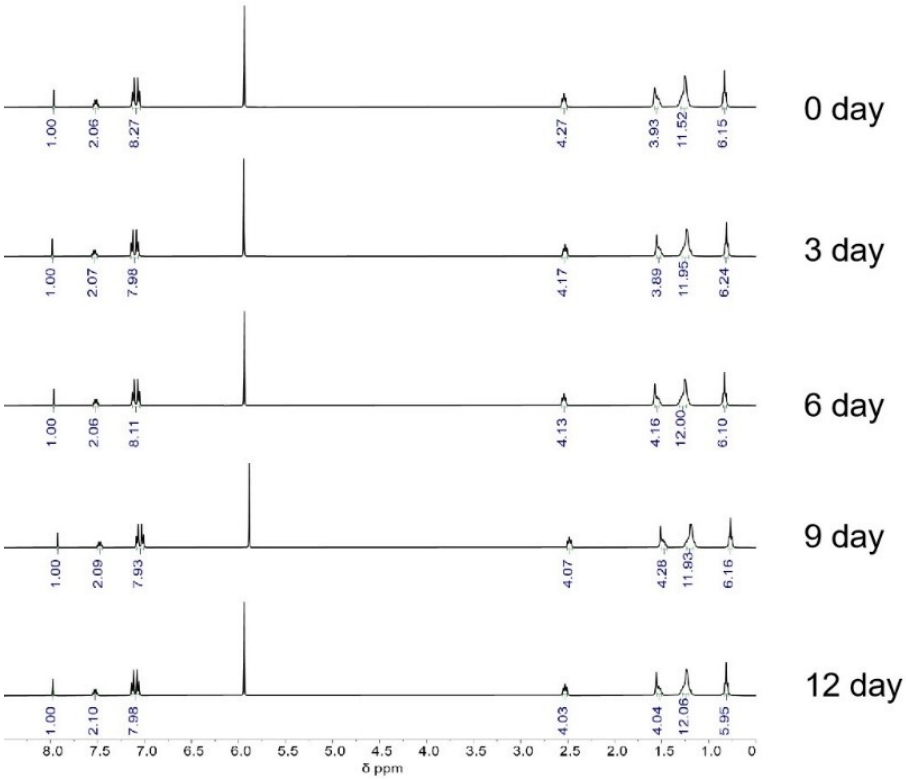

Figure S13. Variable-time ^{1}H NMR spectra of compound **Q4T-4F** (400 MHz, $C_2D_2Cl_4$).

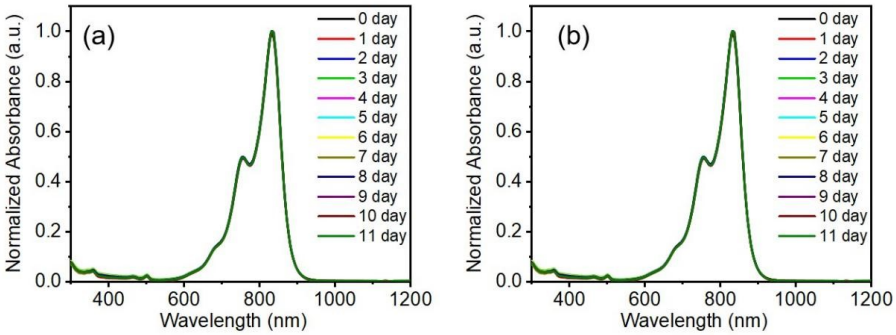

Figure S14. Solution (10^{-5} mol L^{-1} in *o*-DCB) UV-*vis*-NIR absorption spectra of compounds (a) **Q4T** and (b) **Q4T-4F** for different time.

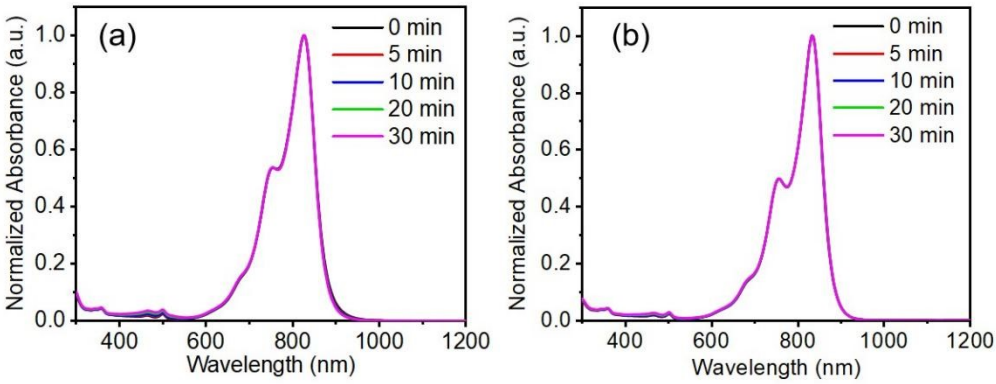

Figure S15. Solution (10^{-5} mol L^{-1} in *o*-DCB) UV-*vis*-NIR absorption spectra of (a) **Q4T** and (b) **Q4T-4F** by UV irradiation for different time.

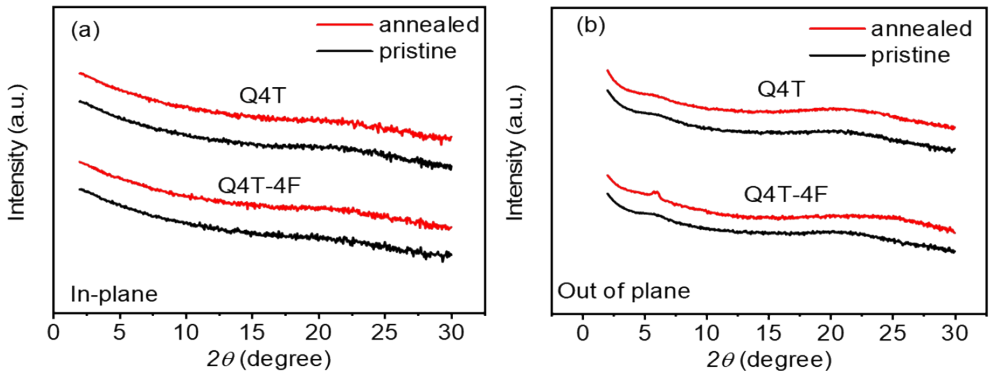

Figure S16. (a) In-plane and (b) out-of-plane film GIXRD patterns of **Q4T** and **Q4T-4F** before and after thermal annealing.

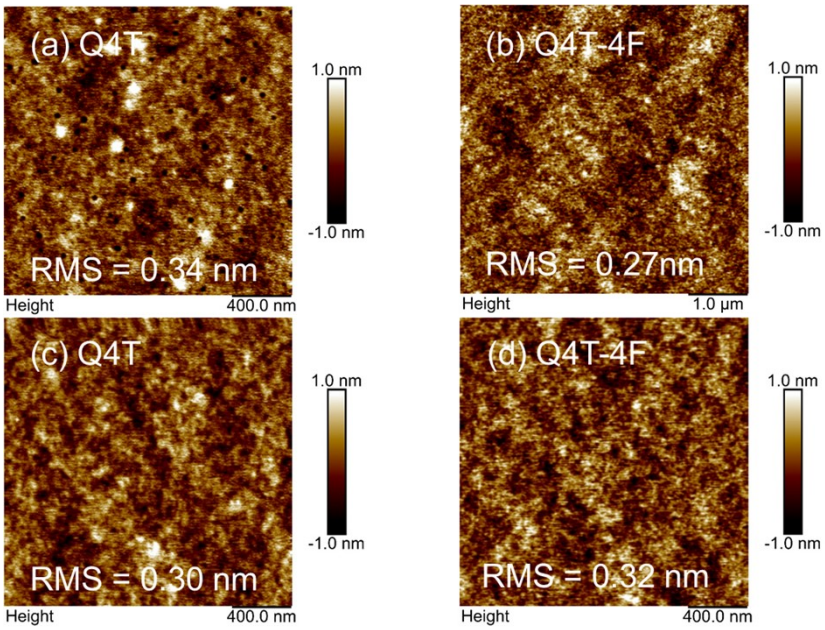

Figure S17. AFM height images (2 µm × 2 µm) of pristine (a) **Q4T** and (b) **Q4T-4F** and annealed (c) **Q4T** and (d) **Q4T-4F** thin films.

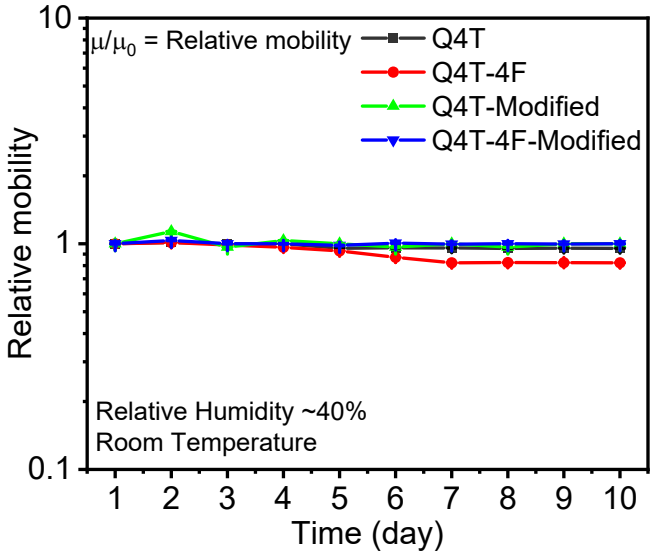

Figure S18. Ambient stability of **Q4T** and **Q4T-4F** based OTFTs stored with a relative humidity of *ca.* 40%.

4. X-ray crystallography

The single crystals of compounds **Q4T** and **Q4T-4F** were grown by diffusion of methanol into their toluene solutions. Single crystals data collections were performed at 213 K for **Q4T** and **Q4T-4F** on a SuperNova diffractometer, using graphite-monochromated Mo Kα radiation (λ = 0.71073 Å. The data were collected on a "Bruker

APEX-II CCD" diffractometer. Using Olex2, these structures were solved with the ShelXT and refined with the ShelXT97 refinement package using Least Squares minimization. Refinement was performed on F^2 anisotropically for all the non-hydrogen atoms by the full-matrix least-squares method. The hydrogen atoms were placed at the calculated positions and were included in the structure calculation without further refinement of the parameters.

Table S1. Crystal data and structure refinement for compound **Q4T**.

Identification code	Q4T	
Empirical formula	C82 H78 O4 S4	
Formula weight	1255.68	
Temperature	213.00 K	
Wavelength	1.34139 Å	
Crystal system	Triclinic	
Space group	P-1	
Unit cell dimensions	a = 14.306(12) Å	α = 94.32(3)°.
	b = 17.755(16) Å	β = 112.18(2)°.
	c = 18.065(16) Å	γ = 96.58(3)°.
Volume	4186(6) $Å^3$	
Z	2	
Density (calculated)	0.996 Mg/m^3	
Absorption coefficient	0.893 mm^{-1}	
F(000)	1332	
Crystal size	0.06 x 0.05 x 0.01 mm^3	
Theta range for data collection	3.386 to 55.418°.	
Index ranges	-17<=h<=17, -21<=k<=21, -19<=l<=21	
Reflections collected	40692	
Independent reflections	15453 [R(int) = 0.1404]	
Completeness to theta = 53.594°	98.8 %	
Absorption correction	Semi-empirical from equivalents	
Max. and min. transmission	0.7508 and 0.3279	
Refinement method	Full-matrix-block least-squares on F^2	
Data / restraints / parameters	15453 / 121 / 815	
Goodness-of-fit on F^2	0.854	
Final R indices [I>2sigma(I)]	R1 = 0.1390, wR2 = 0.3288	
R indices (all data)	R1 = 0.2254, wR2 = 0.4281	
Extinction coefficient	n/a	

Largest diff. peak and hole	0.568 and -0.354 e.Å^{-3}

Table S2. Crystal data and structure refinement for compound **Q4T-4F**.

Identification code	Q4T-4F	
Empirical formula	C82 H68 F4 O4 S4	
Formula weight	1321.60	
Temperature	212.99 K	
Wavelength	1.34139 Å	
Crystal system	Triclinic	
Space group	P-1	
Unit cell dimensions	a = 13.646(3) Å	α = 76.530(10)°.
	b = 16.361(2) Å	β □= 69.642(10)°.
	c = 18.598(4) Å	γ □ = 73.720(9)°.
Volume	3694.3(12) $Å^3$	
Z	2	
Density (calculated)	1.188 Mg/m^3	
Absorption coefficient	1.080 mm^{-1}	
F(000)	1384	
Crystal size	0.08 x 0.01 x 0.01 mm^3	
Theta range for data collection	3.505 to 55.363°.	
Index ranges	-16<=h<=16, -19<=k<=19, -20<=l<=22	
Reflections collected	48613	
Independent reflections	14016 [R(int) = 0.0933]	
Completeness to theta = 53.594°	99.7 %	
Absorption correction	Semi-empirical from equivalents	
Max. and min. transmission	0.7508 and 0.4511	
Refinement method	Full-matrix least-squares on F^2	
Data / restraints / parameters	14016 / 79 / 851	
Goodness-of-fit on F^2	0.891	
Final R indices [I>2sigma(I)]	R1 = 0.0922, wR2 = 0.2035	
R indices (all data)	R1 = 0.1595, wR2 = 0.2466	
Extinction coefficient	n/a	
Largest diff. peak and hole	0.615 and -0.408 e.$Å^{-3}$	

5. References

[1] Gaussian 09; Revision A.2; Frisch, M. J.; Trucks, G. W.; Schlegel, H. B.; Scuseria, G. E.; Robb, M. A.; Cheeseman, J. R.; Scalmani, G.; Barone, V.; Mennucci, B.; Petersson, G. A.; Nakatsuji, H.; Caricato, M.; Li, X.; Hratchian, H. P.; Izmaylov, A. F.; Bloino, J.; Zheng, G.; Sonnenberg, J. L.; Hada, M.; Ehara, M.; Toyota, K.; Fukuda, R.; Hasegawa, J.; Ishida, M.; Nakajima, T.; Honda, Y.; Kitao, O.; Nakai, H.; Vreven, T.; Montgomery, J., J. A.; Peralta, J. E.; Ogliaro, F.; Bearpark, M.; Heyd, J. J.; Brothers, E.; Kudin, K. N.; Staroverov, V. N.; Kobayashi, R.; Normand, J.; Raghavachari, K.; Rendell, A.; Burant, J. C.; Iyengar, S. S.; Tomasi, J.; Cossi, M.; Rega, N.; Millam, N. J.; Klene, M.; Knox, J. E.; Cross, J. B.; Bakken, V.; Adamo, C.; Jaramillo, J.; Gomperts, R.; Stratmann, R. E.; Yazyev, O.; Austin, A. J.; Cammi, R.; Pomelli, C.; Ochterski, J. W.; Martin, R. L.; Morokuma, K.; Zakrzewski, V. G.; Voth, G. A.; Salvador, P.; Dannenberg, J. J.; Dapprich, S.; Daniels, A. D.; Farkas, Ö.; Foresman, J. B.; Ortiz, J. V.; Cioslowski, J.; Fox, D. J.; Gaussian, Inc., Wallingford CT, **2009**.

[2] Becke, A. D. Density‐functional Thermochemistry. III. The Role of Exact Exchange. *J. Chem. Phys.* **1993**, *98*, 5648.

[3] Hehre, W. J.; Ditchfield, R.; Pople, J. A. Self-Consistent Molecular Orbital Methods. XII. Further Extensions of Gaussian-Type Basis Sets for Use in Molecular Orbital Studies of Organic Molecules. *J. Chem. Phys.* **1972**, *56*, 2257.

[4] Yamanaka, S.; Okumura, M.; Nakano M.; Yamaguchi, K. EHF Theory of Chemical Reactions Part 4. UNO CASSCF, UNO CASPT2 and R (U) HF CoupledCluster (CC) Wavefunctions. *J. Mol. Struct.* **1994**, *310*, 205.

[5] Kamada, K.; Ohta, K.; Shimizu, A.; Kubo, T.; Kishi, R.; Takahashi, H.; Botek, E.; Champagne B.; Nakano, M. Singlet Diradical Character from Experiment. *J. Phys. Chem. Lett.* **2010**, *1*, 937.